Molecular Therapy
Oncolytics
Original Article

Applications of nuclear-based imaging in gene and cell therapy: probe considerations

Alessia Volpe,[1] Naga Vara Kishore Pillarsetty,[1,3] Jason S. Lewis,[1,2,3] and Vladimir Ponomarev[1,2,3]

[1]Department of Radiology, Memorial Sloan Kettering Cancer Center, New York, NY, USA; [2]Molecular Pharmacology Program, Memorial Sloan Kettering Cancer Center, New York, NY, USA; [3]Weill Cornell Medical College, New York, NY, USA

Several types of gene- and cell-based therapeutics are now emerging in the cancer immunotherapy, transplantation, and regenerative medicine landscapes. Radionuclear-based imaging can be used as a molecular imaging tool for repetitive and non-invasive visualization as well as *in vivo* monitoring of therapy success. In this review, we discuss the principles of nuclear-based imaging and provide a comprehensive overview of its application in gene and cell therapy. This review aims to inform investigators in the biomedical field as well as clinicians on the state of the art of nuclear imaging, from probe design to available radiopharmaceuticals and advances of direct (probe-based) and indirect (transgene-based) strategies in both pre-clinical and clinical settings. Notably, as the nuclear-based imaging toolbox is continuously expanding, it will be increasingly incorporated into the clinical setting where the distribution, targeting, and persistence of a new generation of therapeutics can be imaged and ultimately guide therapeutic decisions.

Imaging is a quintessential part of gene therapy to understand the localization, extent, and duration of gene expression of target genes.[1,2] Among imaging approaches, radionuclide-based imaging approaches have several advantages such as high sensitivity and no depth limitation, which provides them with the ability to interrogate function of the gene (endogenous or exogenous) without perturbing the system and whole-body readout to understand effects on the target as well as non-target tissue. Single-photon emission computed tomography (SPECT) using gamma-emitting isotopes and positron emission tomography (PET) imaging with positron-emitting isotopes are two widely used modalities both in pre-clinical and clinical settings. SPECT imaging provides three-dimensional tomographic images of radioactivity distribution in the body, taking advantage of gamma rays produced by the decay of radioactive isotopes. PET imaging takes advantage of annihilation of positrons (emitted by decaying radioisotopes) with an electron that results in production of collinear photons of 510 keV that are detected simultaneously to produce a three-dimensional map of radioactive distribution in the body.[3] SPECT is relatively less sensitive, requiring longer scanning times and higher radioactivity administration, but it can provide the ability to conduct simultaneous multitracer studies.[4] While non-radionuclide-based imaging modalities have some ability to provide quantitative information, their wide applicability and clinical utility are very limited due to a number of factors. PET imaging is a quantitative imaging modality with exquisitely high sensitivity and can be used for quantifying gene expression that can aid in temporal assessment of output of gene expression.[5] With advances in multimodality gamma cameras, algorithms for image reconstruction, and compensation techniques to correct for photon attenuation and scattering, SPECT imaging can be quantitative.[6] Therefore, both PET and SPECT imaging can be utilized for developing and optimizing gene therapy approaches in pre-clinical models and translated to the clinic without major barriers to non-invasively measure the efficacy of gene therapy.

Radiochemical probe design and radioisotope considerations

A radiochemical probe, commonly termed as a radiopharmaceutical, is a radiolabeled entity administered to the subject. Placement of the radioisotope must not perturb or interfere with binding/biological properties of the probe toward its biological target. A basic but necessary feature for a radionuclide to be useful for *in vivo* imaging applications is that its decay must lead to a photon with sufficient energy that it can penetrate the body with minimal attenuation and scattering and reach the detectors on the camera to be registered as a signal. Depending on whether the radioisotope is intended for SPECT or PET imaging application, the decay properties that make them ideal are a bit different. The gamma rays emitted by an ideal SPECT isotope are tipically within a usable energy window of 50–200 keV and have a high decay efficiency and low abundance of high-energy gamma rays and particle emissions. The emitted positron of an ideal PET isotope has to have low energy, a high decay efficiency, and a low abundance of concurrent photon emissions in the 450–650 keV energy window and lack other gamma or particle emissions. High positron energy is not ideal because the positron travels much longer distances before annihilating with the electron, thereby creating high uncertainty in determining its position, which leads to reduced image resolution. Generally, short-lived isotopes (half-life [$t_{1/2}$] < 4 h) used for imaging-based applications are produced using in-house cyclotrons or generator systems, while the long-lived isotopes ($t_{1/2}$ > 12 h) can be produced on cyclotrons or linear accelerators (LINACs) or nuclear reactors at a different site and shipped across

Received 11 November 2020; accepted 26 January 2021;
https://doi.org/10.1016/j.omto.2021.01.017.

Correspondence: Vladimir Ponomarev, MD, PhD, Memorial Sloan Kettering Cancer Center, 1275 York Avenue, New York, NY 10065, USA.
E-mail: ponomarv@mskcc.org

Table 1. Radioactive isotopes used for cell labeling

Radioisotopes	Half-life	Imaging modality	Emissions[a]	Production method	Radiolabeling method	Biological vectors
^{11}C	20.3 min	PET	β^+ (99.8%)	cyclotron	covalent	small molecules, peptides
^{13}N	9.97 min	PET	β^+ (99.8%)	cyclotron	covalent	small molecules, peptides
^{18}F	109.8 min	PET	β^+ (96.7%)	cyclotron	covalent and chelator, AlF-NOTA	small molecules, peptides
^{64}Cu	12.7 h	PET	β^+ (17.4%)	cyclotron	chelator-based, DOTA	peptide antibodies, nanoparticles
^{67}Ga	3.25 days	SPECT	γ (93.3 keV, 38.8%; 184 keV, 21.4%; 300 keV, 16.6%)	cyclotron	chelator-based, DOTA, DTPA, HBED	peptide antibodies, nanoparticles
^{68}Ga	68 min	PET	β^+ (88.9%)	generator system	chelator-based, DOTA, DTPA, HBED	small molecules, peptides
^{72}As	26 h	PET	β^+ (87.9%), γ (834 keV, 81.0%; 629 keV, 8.1%)	cyclotron & generator systems	covalent, trithiol chelators	peptide antibodies, nanoparticles
^{76}Br	16.2 h	PET	β^+ (55.1%), γ (559 keV, 74%; 657 keV, 15.9%; 1,854 keV, 14.7%; 1,216 keV, 8.8%; 2,951 keV, 7.4%; 2,793 keV, 5.6%)	cyclotron	covalent	small molecules, peptide antibodies, nanoparticles
^{77}Br	57 h	SPECT	γ (239 keV, 23.1%; 521 keV, 22.4%)	cyclotron	covalent	small molecules, peptide antibodies, nanoparticles
^{89}Zr	3.3 days	PET	β^+ (22.7%), γ (909 keV, 99.0%)	cyclotron	chelator-based, DFO	peptide antibodies, nanoparticles
^{99m}Tc	6 h	SPECT	γ (141 keV, 89.0%)	generator system	chelator-based, N2S2, N3S, and others	small molecules, peptides
^{111}In	67.2 h	SPECT	γ (245 keV, 94.1%; 171 keV, 90.6%)	cyclotron	chelator-based, DOTA, DTPA	peptide antibodies, nanoparticles
^{123}I	13.2 h	SPECT	γ (159 keV, 83.3%)	cyclotron	covalent	peptide antibodies, nanoparticles
^{124}I	4.18 days	PET	β^+ (22.9%), γ (603 keV, 62.9%; 1,691 keV, 11.2%; 723 keV, 10.4%)	cyclotron	covalent	peptide antibodies, nanoparticles
^{125}I	59 days	SPECT	γ (27.5 keV, 6.7%), X-rays	reactor	covalent	peptide antibodies, nanoparticles
^{131}I	8.02 days	SPECT	γ (364 keV, 81.5%; 637 keV 7.2%; 284 keV, 6.1%)	reactor	covalent	peptide antibodies, nanoparticles

[a]Only positron or photons in >5% yield relevant to PET/SPECT.

states or countries depending on the half-life. There are several PET and SPECT isotopes with suitable decay properties that make them good candidates for imaging applications. The general consensus among the imaging community based on the principle of minimizing the radiation dose to the subject is to choose a radioisotope whose half-life is in the same range as the half-life of the radiochemical probe. Therefore, small molecules and peptides that have relatively short biological half-lives are labeled with short-lived isotopes, whereas antibodies and nanoparticles that have long biological half-lives are radiolabeled with longer-lived isotopes. However, depending on the application, the density of the target, and the pharmacokinetics of the probe, these general rules can be changed to develop an optimal imaging probe. Table 1 provides a list of medically useful isotopes and their decay properties, including types of emission and half-life.

While the physical decay properties form the basis of detection, the chemical properties of the radionuclide, its radionuclidic and chemical purity, and its chemical form determine how it can be incorporated into a biological vector. Table 1 also lists the general method on how the radionuclide can be incorporated into the radiochemical probe to facilitate imaging. Covalent attachment to the molecule is the most stable way to incorporate a radionuclide to the radiochemical probe without imparting any charge to the molecule. Carbon-11, nitrogen-13, fluorine-18, bromine-76/77, and iodine-123/124/125/131 are the most commonly used isotopes for such purposes. Because many small molecules (natural products as well as synthetic drugs) contain these elements in their framework, with a suitable chemical approach the stable isotope can be replaced in the radioactive isotope without changing the structure of the molecule. Because these elements can be incorporated directly onto a molecule and do not impart a charge, they can be appended to many small molecules without drastically impacting the structure or the binding of the molecule to its target. While the properties of the resulting radiochemical probes are ideal, the challenge is in developing suitable chemistry that will provide a radiochemically pure compound in high yield, and several seemingly simple small molecules remain inaccessible due to such challenges in chemistry. The most widely used radioisotopes for imaging applications are metals that cannot be directly incorporated onto a molecule. Metals require a chelator (a polydentate binding ligand) that has high affinity for metal to ensure facile incorporation

onto the molecule and high kinetic and thermodynamic stability to ensure *in vivo* stability of the radiochemical probe. Chelators are bulky appendages, and the resulting metal-chelate complexes are not neutral in most cases and impart charge to the molecule. Therefore, metal chelates are most commonly used for incorporating radiometals to peptides, antibodies, and nanoparticles. Due to the ease of labeling and high stability of the resulting complexes, radiometals are most extensively used in the clinic as well as for developing new radiochemical probes.[7] These are the general considerations for choosing a particular radioisotope for labeling a molecule that can act as an imaging probe for gene therapy applications.

Direct and indirect cell labeling do offer whole-body non-invasive tracking capabilities both preclinically and clinically. Herein, we discuss the existing and emerging applications of nuclear imaging using direct and indirect approaches in (1) gene therapy and (2) cell-based therapies.

Direct versus indirect imaging

Gene expression imaging using radionuclide-based probes can be performed using direct or indirect approaches.[8] The direct approach involves developing a radiochemical probe that interacts directly with the gene product introduced using gene therapy and localizes in a cell in a concentration-dependent manner. This type of approach is applicable when the target gene product is an enzyme, transporter, or a neo-antigen that is unique to the target cell.[9] Radiolabeled probes can act as substrates for enzymes or transporters or as proteins or molecules with high-affinity binding to the unique target antigen. However, gene therapy can involve introducing a gene product that is not targetable/easily accessible (e.g., nuclear or mitochondrial proteins, single nucleotide variants) or gene silencing. In such scenarios a surrogate gene, also called as reporter gene (e.g., herpes simplex virus type 1-thymidine kinase [HSV1-*tk*], norepinephrine transporter [NET], sodium iodide symporter [NIS]), that can be targeted using a radiochemical probe can be expressed as a fusion protein or as a separate protein using bi- or multi-cistronic vectors that will ensure a stoichiometric expression of the gene product.[10–14] For gene therapy involving RNAi technology, direct labeling of RNAi with a suitable radiolabeled conjugate can provide information about the delivery of the vector.[15] Irrespective of the type of imaging approach, the design, function, and pharmacokinetic behavior of the radiochemical probe is the most crucial determinant in ensuring that the signal obtained using the radiochemical probe directly correlates to the efficacy of gene therapy.

Direct labeling of cells: principles and considerations

Direct labeling uses *ex vivo* labeling of cells prior administration into animal models and/or humans. Labeling can be performed artificially, by incubating cells with a wide number of ready-to-use contrast agents. This method has been successfully applied to track a variety of cell types.[16–20] Some labels are introduced into cells by a lipophilic chelator and subsequent binding to intracellular proteins, while the chelator leaves the cell. Transfection agents are also used to help the label enter the desired cells. They are usually cationic molecules, polymers, or liposomes/lipoplexes with positively charged head groups that neutralize the plasma membrane electrostatic charge by interacting with the negatively charged phospholipids in the inner layer. Another method is based on electroporation. This technique enables the passage of the cell label through the cell membrane by increasing its permeability.

Cells can also be *ex vivo* labeled by exploiting their cellular processes (e.g., receptor-mediated internalization, phagocytosis). Macrophages can be successfully marked via their phagocytic function and used to depict tumor-associated macrophage (TAM) infiltration at the tumor[21,22] or active migration to inflammatory lesions.[23–25] Cells are incubated with the desired imaging agent and then washed multiple times to remove the unlabeled radiotracer. Radioactivity of cells and washes is measured using an automated gamma counter. Cell-labeling efficiency (LE [%]) depends on both labeling conditions and cell type. It is calculated as follows:

$$LE(\%) = \left(\frac{activity\ of\ cell\ fraction}{activity\ of\ cell\ fraction + activity\ of\ combined\ washes}\right) x100. \quad (1)$$

Once cells are successfully labeled *in vitro*, they can be injected into a living animal. The imaging agent used to label them can be lost over time due to efflux or dilution.

When efflux occurs and the leaked isotope is not immediately excreted, its redistribution generates background, rendering it impossible to distinguish between labeled cells and free isotope. Notably, as the cells continue to actively divide, the label is distributed to the progeny and is progressively diluted. The overall signal strength is maintained for a variable amount of time until radiotracer decay (which depends on the half-life of the radiotracer being used), but cell expansion is not detectable as the number of individually labeled cells decreases.[26] This limitation makes direct labeling particularly unsuitable for long-term observation of fast-growing cells (e.g., cancer cells or expanding T cells). To compensate for signal loss due to decay, radioisotopes with a longer half-life can be used for both PET and SPECT. A list of radioisotopes and respective radiolabeled probes can be found in Table 2.

SPECT isotopes for direct labeling of cells

^{111}In-oxine ($t_{1/2}$ = 67.2 h; EC/γ) is being used in models of myocardial infarction to identify endothelial progenitor cells,[27] hematopoietic stem cells,[28] and cardiomyoblasts[29] in less perfused areas. *In vivo* monitoring of ^{111}In-oxine-labeled cytotoxic T lymphocytes (CTLs) revealed that lymphodepletion combined with adoptive transfer of CTLs increases their recruitment at the tumor site and improves anti-tumor efficacy in a xenograft model of colon cancer (Figure 1A).[30] In an in-human study, antigen-loaded dendritic cells labeled with ^{111}In-oxine were injected intradermally in patients with different types of cancer (i.e., melanoma, colorectal cancer, lung cancer, and myosarcoma).[31] ^{99m}Tc-HMPAO ($t_{1/2}$ = 6.02 h; 99% γ) imaging was used

Table 2. Radioactive probes for direct cell labeling

Modality	Radioactive isotope	Radiopharmaceutical probe	Half-life	Distribution and properties
SPECT	^{111}In	^{111}In-oxine	67.2 h	liver, spleen, bone marrow; only transient pulmonary uptake; tracer crosses blood-brain barrier (BBB)
	^{99m}Tc	[^{99m}Tc]HMPAO	6.02 h	spleen, liver, kidneys, bone marrow, and bowel; hepatobiliary and renal excretion; lipophilic tracer (crossing the plasma membrane); it crosses the BBB
PET	^{18}F	[^{18}F]FDG	109.7 min	in metabolically active organs (brain, heart, kidneys, liver); after a few hours, it is mainly found in kidneys and bladder due to its renal excretion; other sites of physiological uptake are skeletal muscles, brown fat, gastrointestinal mucosa, salivary glands, lactating breasts, and hematopoietic/lymphoid tissues (including thymus, spleen and bone marrow); tracer crosses BBB
	^{64}Cu	[^{64}Cu]PTSM	12.7 h	main distribution in the liver, as the radiotracer is predominantly metabolized by hepatocytes; distribution also in the large intestine and pancreas; minimal activity in the lungs; tracer does not cross BBB
	^{89}Zr	^{89}Zr-oxine, ^{89}Zr-DBN	3.3 days	mainly in the liver; as a result of demetallation, free ^{89}Zr predominantly accumulates in bones, joints, and marrow because of its high affinity for electronegative donor atoms (i.e., oxygen and phosphorus) in hydroxyapatite present in the bone matrix; tracer does not cross BBB

to determine neutrophil recruitment in inflamed areas of a colitis model[32] as well as for labeling autologous white blood cells in mouse models of infectious disease.[33] Lukawska et al.[34,35] monitored the distribution pattern of eosinophils and neutrophils pre-labeled with ^{99m}Tc-HMPAO in asthmatic patients. ^{99m}Tc-HMPAO typically shows bowel activity owing to hepatobiliary secretion, rendering it less suitable for *in vivo* tracking in the abdominal cavity (Figure 3B).[33]

PET isotopes for direct labeling of cells

^{18}F-FDG ($t_{1/2}$ = 109.7 min; 97% β^+) has been used to label *ex vivo* a variety of cells;[36–38] however, this is not a suitable tracer for the imaging of low metabolically active cells, while the short half-life restricts its application to short-term studies (a few hours). The longer half-life of ^{64}Cu ($t_{1/2}$ = 12.7 h; 18% β^+) compared to ^{18}F allows cells to be tracked for approximately 2–3 days with PET. ^{64}Cu-PTSM was used to efficiently label C6 rat glioma cells (70%–85% uptake at 5 h), but it showed a significant efflux rate already 24 h after labeling,[16] similar to ^{111}In. However, while ^{111}In is rapidly excreted through the kidneys,[39] ^{64}Cu accumulates mainly in the liver, followed by the large intestine and pancreas,[40] generating undesirable background. As both ^{18}F and ^{64}Cu have significant limitations, ^{89}Zr ($t_{1/2}$ = 78.4 h; 23% β^+) was developed as a PET equivalent of ^{111}In, showing promising labeling and retention in cells and allowing tracking for up to 2 weeks. Human mesenchymal stem cells were covalently labeled with ^{89}Zr-DBN.[17] More recent studies successfully used ^{89}Zr-oxine for direct labeling of adoptively transferred natural killer (NK) cells and dendritic cells,[41] chimeric antigen receptor (CAR) T cells,[42,43] and gamma-delta T cells,[44] supporting the translation of this methodology into humans for monitoring the *in vivo* distribution of cell-based immunotherapies (Figure 1B).

Pros and cons of direct cell labeling

Direct labeling of cells is an easy procedure involving exposure of the cells to (1) a radiometal complex resulting in cellular uptake via diffusion or transport-mediated mechanisms, or (2) by electrostatically or covalently binding the radioisotope onto the cell surface. Some clinically-compatible radiotracers used for *ex vivo* labeling can have a direct impact on cell viability and function. Botti et al.[45] demonstrated that ^{111}In-oxine and ^{18}F-FDG achieve a greater labeling efficiency than does ^{99m}Tc-HMPAO in T cells, but they are responsible for a progressive reduction of their proliferative ability, with cell death occurring 8–9 days after labeling, and impaired cytotoxic function.

Importantly, together with the already discussed issues related to label efflux and dilution, the direct labeling approach does not provide viability information on the cells, as dead cells will still lead to signal, thereby impacting the biological interpretation of the generated data. Indirect cell labeling approaches can overcome many of the above challenges associated with direct labeling and are discussed in the following section.

As the *ex vivo* labeling process does not involve genetic manipulation of the cells, a few regulatory hurdles for clinical application have to be overcome, rendering this approach easily translatable into patients for short-term monitoring of cells and therapeutics.

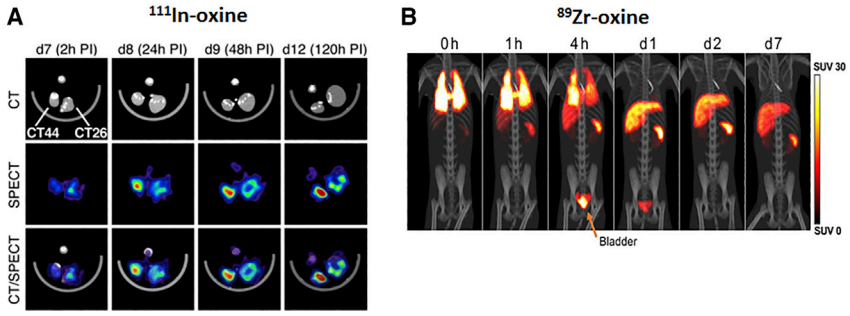

Figure 1. Application of preclinical direct nuclear imaging in cell therapy

(A) CT, SPECT, and SPECT-CT images obtained at 2, 24, 48, and 120 h after ^{111}In-oxine-labeled hemagglutinin (HA)-specific CTL administration. CT44 HA^{+} and CD26 HA^{-} colon tumors were established in the right and left footpad, respectively. Directly labeled cells using ^{89}Zr-oxine in rhesus macaques is shown. (B) PET-CT of autologous ^{89}Zr-oxine-labeled NK cells was performed after infusion and treatment with deferoxamine. Adoptive NK cell trafficking was monitored for up to 7 days and showed initial localization to the lungs, followed by a progressive distribution in liver and spleen. Bladder uptake is due to renal excretion of free ^{89}Zr being released from dead/dying cells and chelated by deferoxamine. All figures adapted with permission from publishers.

Indirect labeling: principles and considerations

Indirect labeling requires genetic engineering of cells to ectopically express a reporter gene and ensure its genomic integration and long-term expression.

Once a suitable expression cassette is designed, reporter genes are ectopically introduced to cells using (1) viral vectors (retroviral, adenoviral, and lentiviral based), (2) episomal plasmids (transposons), or through (3) gene editing.

Reporter gene-expressing cells are expanded i*n vitro* and tested for radioactive uptake. Cellular radiotracer uptake is expressed as % uptake and calculated as follows:

$$\%Uptake = \left(\frac{counts(cells)}{counts\ (cells) + counts\ of\ combined\ washes}\right) x100. \quad (2)$$

Cells are then injected in the desired living organism, including humans. Following the systemic administration of a suitable labeling agent, the reporter gene is *in vivo* targeted by molecular imaging. A variety of radiolabeled probes for both PET and SPECT were developed to image specific tumor types and are already clinically approved. They accumulate where certain endogenous receptors or transporters are highly expressed. The same probes can therefore be used to image human-derived reporter genes (such as [^{111}In]DTPA-octreotide for SSTR2[46] and [^{123}I]- or [^{131}I]MIBG for NET[47,48]).

Conventionally, reporter genes are classified as (1) transporters, (2) receptors, or (3) enzymes. A comprehensive list of radionuclide-based reporter genes and corresponding imaging probes can be found in Table 3.

Indirect imaging in gene therapy

Oncolytic viruses have emerged in the landscape of gene therapy,[49,50] and their application to treat a variety of tumor types is currently being investigated in preclinical studies using non-invasive imaging strategies. As HSV vectors proved to be successful in the treatment of several cancers,[51–56] it is paramount to monitor their distribution, delivery, and replication. Bennett et al.[57] showed the feasibility of [^{124}I]FIAU-afforded PET to image HSV1 oncolytic virus with thymidine kinase in a model of human colorectal cancer. This was the first study to report time- and dose-dependent replication of an oncolytic virus. [^{18}F]FHBG (9-[4-fluoro-3-(hydroxymethyl)butyl]guanine)-afforded PET was used to monitor adenoviral-mediated HSV1-*tk* transgene expression in patients with hepatocellular carcinoma.[58] In addition to serving as a reporter gene, HSV1-*tk* was also used as a gene therapy against the tumor. In fact, the kinase is able to convert ganciclovir (orally administered into patients) into a cytotoxic compound, thereby inducing cancer cell death with a bystander effect.[58,59]

NIS has also been used in a number of gene therapy studies.[60–66] The first reported study with NIS was from Merron et al.[67] The authors incorporated NIS into two different oncolytic adenoviruses (AdlP1 virus based on the adenovirus serotype 5, and AdAM6 virus, encoding for the hTR promoter driving the expression of the E1 region) to study their *in vivo* distribution in colorectal tumor xenografts by $^{99m}TcO_4$−-afforded SPECT (Figure 1A). In an approach called radio-virotherapy, Dingli et al.[62] also demonstrated that delivering ^{131}I to NIS-expressing viruses amplified their potency against infected tumors. The same principle was applied by Dingli et al.[68] to amplify tumor targeting and anti-cancer activity of therapeutic ^{131}I by gene transfer in a model of multiple myeloma.

Indirect imaging in cell therapy

Nuclear imaging is actively used for monitoring the trafficking, homing, and persistence of cell-based therapies, including adoptive T cells[41,43,44,69–72] and stem cells.[73–76]

Here, we report relevant studies where direct labeling or multiple reporter gene types have been applied for the *in vivo* monitoring of cell-based cancer immunotherapies.

In 2003, Koehne et al.[77] were the first to demonstrate the feasibility of long-term *in vivo* monitoring of cytolytic T cells (CTLs) by HSV1-*tk* reporter-based imaging with [^{131}I]FIAU and [^{124}I]FIAU. Later, Dobrenkov et al.[14] demonstrated the feasibility of monitoring the

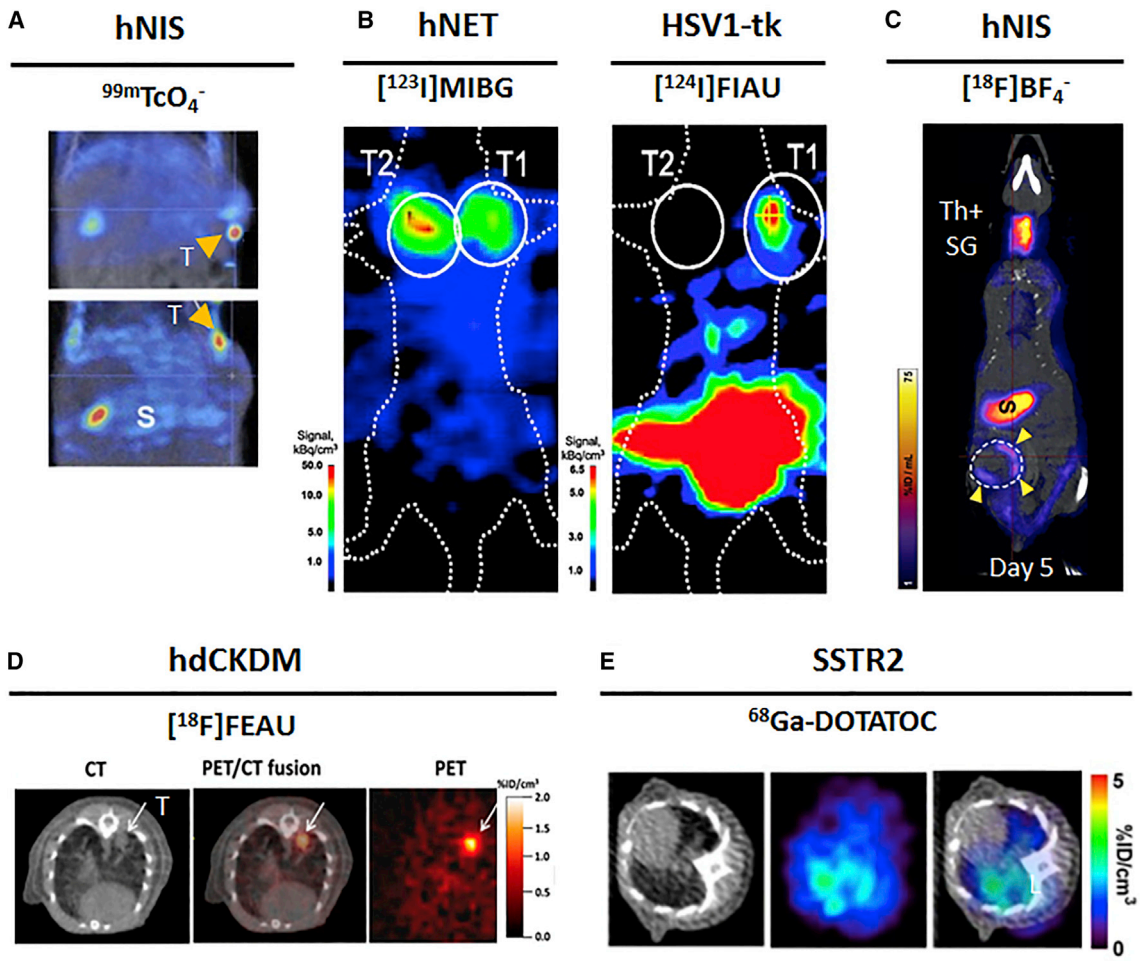

Figure 2. Application of preclinical reporter-based nuclear imaging in cell therapy

Preclinical imaging of cell-based immunotherapies with multiple host-compatible reporter genes and their corresponding radioisotopes. (A) NIS-based $^{99m}TcO_4^-$ imaging of AdIP1 (top) and AdAM6 (bottom) adenoviruses in a HCT116 colorectal carcinoma xenograft. T, tumor; S, stomach. (B) Dual-modality PET-SPECT imaging with [^{123}I]MIBG and [^{124}I]FIAU to visualize intratumorally injected hNET-CD4$^+$ and HSV1-*tk*-CD8$^+$ T cell subpopulations in a human EBV lymphoma xenograft. (C) NIS-based [^{18}F]BF_4^--afforded PET reveals CAR T cell retention differences in two models of TNBC. Endogenous NIS expression, prevalently in thyroid and stomach, does not interfere with imaging. ThSG, thyroid+salivary gland; S, stomach; yellow arrows indicate CAR T cells homing at the tumor. (D) High accumulation of dCKDM/GFP-expressing T cells is observed at the tumor site of treated mice through [^{18}F]FEAU PET imaging. The region of interest is marked by the arrow. (E) Longitudinal PET-CT scan of SSTR2-expressing CAR T cells using ^{68}Ga-DOTATOC. CAR T cells were administered. Indicated images are from the lungs at day 20 after tumor establishment. L, lungs. All figures adapted with permission from publishers.

HSV1-*tk*-transduced CAR-T cell therapy with [^{18}F]FEAU. A comparison of the latter viral reporter with three human-derived reporters (*i.e.*, NIS, NET, and dCK) and corresponding tracers was carried out by Moroz et al.[72] The mutant version of HV1-*tk* (HSV1-sr39*tk*) paired with [^{18}F]FEAU was also used by Dotti et al.[78] to detect autologous polyclonal macaque CTLs after their intravenous infusion in non-human primates.

A dual-reporter imaging study from Doubrovin et al.[79] allowed simultaneous tracking of two distinct EBV-specific T cell subpopulations, using the non-immunogenic human NET and HSV1-*tk* to visualize CD4$^+$ T and CD8$^+$ T cells with [^{123}I]MIBG-SPECT and [^{124}I]FIAU-PET, respectively (Figure 2B).

NIS-afforded imaging informed the distribution and retention of pan-ErB family-targeted CAR T cells in a model of triple-negative breast cancer (TNBC),[80] using the non-toxic, NIS-specific [^{18}F]BF_4- PET radiotracer (Figure 2C).[81] Following up on the development of a mutated human deoxycytidine kinase by Likar et al.,[69] this reporter has been used in a number of studies, including the *in vivo* detection of CAR-T cells with [^{18}F]FEAU[69] and tumor infiltration by T cells with [^{18}F]FMAU[70] suggesting that hdCK mutants can

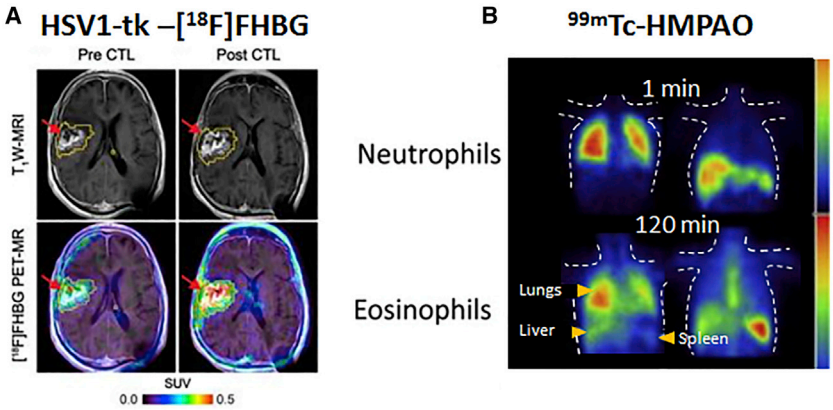

Figure 3. Clinical application of radionuclide-based imaging using indirect and direct strategies

(A) HSV1-*tk* reporter paired with [^{18}F]FHBG PET radiotracer was successfully used for the non-invasive detection of cytolytic CAR-T cells in patients with recurrent glioma. T_1W-weighted (T_1W) MRI was used to assess tumor extent before and after intratumoral CAR-T cell administration (top), and images were superimposed with [^{18}F]FHBG PET (bottom). (B) Dynamic SPECT showing the distribution of ^{99m}Tc-HMPAO-labeled neutrophils and eosinophils in a healthy volunteer. Accumulation of the two cell types appears to be different over time and mainly in lungs, liver, and spleen. All figures adapted with permission from publishers.

be applied for the whole-body clinical detection of immunotherapeutic cells (Figure 2D). Vedvyas et al.[71] chose the SSTR2 reporter gene to study the dynamics of CAR T cells targeting ICAM-1 using the clinically approved ^{68}Ga-DOTATOC PET radiotracer (Figure 2E).

Inducible reporter systems, and sensitivity to T cell activation, can also be used. One notable study from Ponomarev et al.[82] used HSV1-*tk*-reporter-based [^{124}I]FIAU-afforded PET to image nuclear factor of activated T cells (NFAT)-mediated activation of T cells. The *in vivo* monitoring of adoptive T cells functional status can be readily translated into clinical practice by using an alternative non-immunogenic reporter system.

Main studies using nuclear imaging in transplantation and regenerative medicine are here briefly described. Mayer-Kuckuk et al.[83] followed skeletal engraftment of transplanted bone marrow cells by HSV1-*tk*-based [^{18}F]FEAU] PET. The NIS-SPECT approach allows non-invasive imaging and quantification of transduced cardiomyocytes in cardiac transplantation with ^{123}I(74) as well as cardiovascular molecular therapy monitoring with both ^{123}I and $^{99m}TcO_4-$.[73] The same reporter was used in combination with $^{99m}TcO_4-$ to render traceable human-induced pluripotent stem cells during differentiation into hepatocyte-like cells.[76] A study from Witte and colleagues[70] described human hematopoietic stem cell long-term engraftment using the human dCK mutant reporter coupled with a [^{18}F]FMAU PET probe.

Several radiolabeled probes have been developed for clinical HSV1-*tk* PET imaging,[84–90] including FHBG for imaging of the mutated HSV1sr39-*tk*; the pharmacokinetics and dosimetry of [^{18}F]FHBG proved to be safe in healthy volunteers.[91]. However, in a comparative study, Tjuvajev et al.[92] showed that FIAU has a greater sensitivity and a lower abdominal noise over FHPG and FHBG for the *in vivo* imaging of wild-type HSV1-*tk* expression by PET.

Following up on Peñuelas and colleagues,[58] the Gambhir group[93,94] in Stanford successfully used HSV1-*tk* for the non-invasive detection of CD8$^+$ cytolytic CAR-T cells with [^{18}F]FHBG after infusion into the median left front lobe tumor of glioma patients (Figure 3A). Notably, these were the first documented studies of reporter gene-based imaging of cell-based immunotherapies in patients.

Pros and cons of indirect imaging

Reporter genes are a powerful tool for non-invasive and repetitive visualization of biological processes (e.g., gene expression, post-transcriptional events, protein function, protein-protein interaction, enzyme function) in living organisms, including humans. They can be used to improve the diagnosis, develop and monitor new therapeutics (including cell-based therapies and antibodies), and most of their paired radiotracers are already clinically approved.

When choosing a reporter gene for an imaging application, a few considerations have to be made to ensure a favorable imaging contrast. To achieve better contrast, so-called "foreign" reporters are a better suit, as they are nowhere expressed in the body and do not generate background signal (e.g., the PET reporter HSV1-*tk*).[10,87,95] However, because of their physical properties (including radioactive decay), *in vivo* distribution, and the impossibility to modulate them, certain radiolabeled probes can create noise. This can be avoided if the reporter gene is an enzyme catalyzing the conversion of a substrate in a detectable signal (e.g., BLI reporters, not discussed in this review). A downside of foreign reporters is that cells presenting them (e.g., via major histocompatibility complex [MHC] class I or II) can elicit a host immune response.

Host-compatible reporters can be used to avoid the potential risk of immunogenicity, as they come from the same species as the host. However, their endogenous expression in selective tissues could represent an issue in ensuring a favorable contrast in the adjacent organs.

Compared to direct labeling approaches, the permanent integration of the reporter into the genome does not result in label dilution during cell division, and cells can therefore be imaged during their entire lifetime.[96] Since the reporter is passed onto the daughter cells, long-term imaging of expanding cells is also permitted.

Table 3. Reporter genes and corresponding radionuclide imaging agents

Class	Radiopharmaceutical probe	Sites of endogenous expression	Properties
Transporter	Sodium iodide symporter (NIS, SLC5A5)		
	PET: $^{124}I^-$, $[^{18}F]BF_4^-$, $[^{18}F]SO_3F^-$, $[^{18}F]PF_6^-$; SPECT: $^{99m}TcO_4^-$, $^{123}I^-$	thyroid glands, stomach, small intestine, lacrimal glands, lactating mammary glands, choroid plexus, testicles	Na^+ symport alongside various anions; several tracers clinically approved, most not requiring a cyclotron ($^{99m}TcO_4^-$, $^{xyz}I^-$) or made by automated synthesis; tracers do not cross BBB
	Norepinephrine transporter (NET)		
	PET: [^{124}I]MIBG, [^{18}F]MIBG, [^{18}F]PFBG, [^{11}C]hydroxyephedrine; SPECT: [^{123}I]MIBG	organs with central and peripheral sympathetic innervation (brain, heart)	NaCl-dependent monoamine transporter; tracers do not cross BBB
	Dopamine transporter (DAT)		
	PET: [^{11}C]CFT, [^{11}C]PE2I, [^{18}F]FP-CIT; SPECT: [^{123}I]-β-CIT, [^{123}I]-FP-CIT, [^{123}I]-ioflupane, ^{99m}TRODAT	dopaminergic areas of the brain (striatum, substantia nigra, ventral tegmental area)	NaCl-dependent transport; tracers do cross BBB
	Pyruvate kinase M2		
	PET: [^{18}F]DASA-23	central nervous system (CNS), lungs, liver, colon, thyroid, kidneys, bladder and several tumor types (breast, gastric, and colorectal)	suggested for CNS imaging; tracers do cross BBB
Cell surface receptor	Somatostatin receptor type 2 (SSTR2)		
	PET: [^{68}Ga]-DOTATOC, [^{68}Ga]-DOTATATE; SPECT: [^{111}In]-DOTA-BASS, [^{111}In]-DTPA-octreotide; [^{99m}Tc]demotate 1, [^{99m}Tc]P829, [^{188}Re]P829	brain, adrenal glands, gastrointestinal tract, kidneys, spleen, tumors (i.e., pituitary, neuroendocrine, SCLC, pancreatic, paraganglioma, medullary thyroid carcinoma, pheochromocytomas)	G protein-coupled receptor; tracers responsible for cell signaling, change in proliferation, and might impair cell function; non-metal octreotide can cross the BBB; some radiotracers already in use in the clinics (i.e., ^{111}In- and ^{68}Ga-based)
	Dopamine receptor (D_2R) and mutant (D_2R80A)		
	PET: [^{18}F]FESP, [^{11}C]raclopride, [^{11}C]N-methylspiperone	striatum and pituitary gland	G protein-coupled receptor; slow clearance observed for [^{18}F]FESP; tracers do cross BBB
Cell surface antigen	Human carcinoembryonic antigen (CEA)[a]		
	PET: [^{124}I]-anti-CEA scFv-Fc H310A antibody fragment, [^{18}F]FB-T84.66 diabody; SPECT: [^{99m}Tc]-anti-CEA Fab′, [^{111}In]-ZCE-025, ^{111}In-anti-CEA F023C5i[a]	not expressed in healthy adults, with the exception of colon lumen; overexpressed in pancreatic, gastric, colorectal and medullary thyroid cancers	[^{99m}Tc]-anti-CEA Fab′ is FDA approved; tracers do not cross BBB
	DOTA antibody reporter 1 (DAbR1, 2D12.5/G54C), C8.2.5		
	PET: for DAbR1 [^{86}Y]-AABD, [^{177}Lu]-AABD	N/A	murine-derived scFv anti-DOTA IgG1 antibody fused to human CD4 TM domain; DOTA-complex tracer irreversibly binds to the cysteine residue (G54C) of the antibody; tracers do not cross BBB
Cell surface protein	Glutamate carboxypeptidase 2 (PSMA, FOLH1) and variants (tPSMA^{N9Del}, tPSMA^{W2G})[a]		
	PET: [^{18}F]DCFPyL, [^{18}F]DCFBC; SPECT: [^{125}I]DCFPyL; anti-PSMA antibodies and ligands can be flexibly labeled, e.g., J591-IR800	prostate, salivary glands, kidneys	anti-PSMA antibodies and ligands can be flexibly labeled, e.g., J591-IR800; risk of *in vivo* deiodination for radio-iodinated tracers, resulting in uptake in NIS-expressing organs; tracers do not cross BBB
Artificial cell surface molecule	Anti-PEG Fab fragment[a]		
	PET: ^{124}I-PEG-SHPP	N/A	PEG is not toxic and is approved by the FDA; risk of *in vivo* deiodination for radio-iodinated tracers
	Human estrogen receptor α ligand binding domain (hERL)		
	PET: [^{18}F]FES	uterus, ovaries, and mammary glands	does not report on cellular function; tracer is clinically used but does cross the BBB

(*Continued on next page*)

Table 3. *Continued*

Class	Radiopharmaceutical probe	Sites of endogenous expression	Properties
Enzyme	hmtk2 and mutants (hΔTK2, N93D/L109F)		
	PET: [^{124}I]FIAU, [^{18}F]FEAU, [^{18}F]FMAU (hTK2-N93D/L109F)	all tissues (mitochondrial expression); hΔTK2 mutant expressed in the cell cytoplasm; high expression in gall bladder, intestine, and organs involved in clearance	cellular tracer trapping; tracers do not cross the BBB
	hdCK		
	PET: [^{124}I]FIAU, [^{18}F]FEAU	gall bladder, intestine, and organs involved in clearance	cellular tracer trapping; tracers do not cross the BBB
	HSV1-*tk* and mutants (HSV1-sr39tk and HSV1-A167Ytk)		
	PET: [^{124}I]FIAU, [^{18}F]FEAU, [^{18}F]FHBG; other tracers are: [^{18}F]FCAU, [^{18}F]FBAU, [^{18}F]FFEAU, [^{18}F]FMAU, [^{18}F]FHBT	N/A	non-mammalian kinase, potentially immunogenic; tracers do not cross the BBB, unless the latter is compromised; high activity in organs involved in clearance; kinase causes cellular tracer trapping and displays suicide gene properties
	β-galactosidase		
	PET: 2-(4-[^{123}I]iodophenyl)ethyl-1-thio-β-D-galactopyranoside, 3- (2′-[^{18}F]fluoroethoxy)-2-nitrophenyl-β-D- galactopyranoside, 3- [^{11}C]methoxy-2-nitrophenyl-β-D-galactopyranoside, [^{18}F]FPyGal; SPECT: 5-[^{125}I]iodoindol-3-yl-β-D- galactopyranoside ([^{125}I]IBDG)	N/A	glycoside hydrolase encoded by LacZ and isolated from *E. coli*; cellular toxicity may change with substrate; [^{125}I]IBDG has a very fast clearance if systemically administered

FDA, US Food and Drug Administration; IgG1, immunoglobulin G1; N/A, not applicable; PSMA, prostate-specific membrane antigen; scFv, single-chain variable fragment; SCLC, small cell lung cancer; TM, transmembrane; tPSMA, truncated PSMA.
[a]Compatibility with other imaging modalities provided that a suitable contrast forming moiety will be attached (CEA and PEG antibodies, respectively).

While the observation time of directly labeled cells is also influenced by the radiotracer half-life, for indirectly labeled cells that is not the case. As a result, short-lived isotopes are also used and typically dictate the imaging intervals. The genetic engineering approach circumvents complex *ex vivo* labeling procedures and the potential of associated radio damage and toxicity. Reporter gene expression is a prerequisite for radiotracer uptake. As the expression only occurs in viable cells, the resulting signal can be directly attributed to them, thus not only reporting on the presence and distribution of cells, but also providing information on viability and, depending on the reporter of choice, cell function.

The versatility of reporter gene imaging is in part due to the flexibility to tailor the expression cassette to the individual needs. In fact, the reporter gene can be placed under the control of a specific promoter driving its expression, and that can either be a constitutive promoter (e.g., CMV, PGK, LTR)[97] or an inducible promoter. The latter is placed under a particular transcriptional control, therefore linking the reporter gene expression to a particular biological phenomenon.[82,98] However, the complex protocols for genetic engineering (often involving the use of viral reporters), the potential for immune rejection, and the need of a well-established nuclear medicine infrastructure have significantly slowed down their clinical translation.

Final considerations

As current nuclear imaging of gene and cell therapy applications focus primarily on the assessment of therapeutic efficacy and prediction of the response in patients, it will likely become increasingly important in the clinical setting. Importantly, more types of gene and cell therapies are currently emerging in other fields than just cancer immunotherapy (i.e., in transplantation and regenerative medicine).

With expansion of the current imaging toolbox in preclinical and clinical assessment of emerging genetic therapies, future areas of research comprise new radiotracer development for both direct and indirect nuclear imaging. With the advent of total-body PET[99] and hybrid scanners (e.g., PET-MRI),[100,101] low-dose, repetitive nuclear imaging will allow for continuous monitoring of gene therapeutics.

ACKNOWLEDGMENTS

This work was supported by an NIH/NCI Cancer Center Support Grant to MSKCC (P30 CA008748) and by NIH/NCI R35 CA232130 (to J.S.L.).

AUTHOR CONTRIBUTIONS

Conceptualization, A.V., J.S.L., N.V.K.P., and V.P.; writing – original draft, A.V., J.S.L., N.V.K.P., and V.P..

DECLARATION OF INTERESTS

The authors declare no competing interests.

REFERENCES

1. Blasberg, R.G., and Tjuvajev, J.G. (2003). Molecular-genetic imaging: current and future perspectives. J. Clin. Invest. *111*, 1620–1629.
2. Peñuelas, I., Haberkorn, U., Yaghoubi, S., and Gambhir, S.S. (2005). Gene therapy imaging in patients for oncological applications. Eur. J. Nucl. Med. Mol. Imaging *32* (*Suppl 2*), S384–S403.
3. Vaquero, J.J., and Kinahan, P. (2015). Positron emission tomography: current challenges and opportunities for technological advances in clinical and preclinical imaging systems. Annu. Rev. Biomed. Eng. *17*, 385–414.
4. Khalil, M.M., Tremoleda, J.L., Bayomy, T.B., and Gsell, W. (2011). Molecular SPECT imaging: an overview. Int. J. Mol. Imaging *2011*, 796025.
5. Basu, S., Kwee, T.C., Surti, S., Akin, E.A., Yoo, D., and Alavi, A. (2011). Fundamentals of PET and PET/CT imaging. Ann. N Y Acad. Sci. *1228*, 1–18.
6. Bailey, D.L., and Willowson, K.P. (2013). An evidence-based review of quantitative SPECT imaging and potential clinical applications. J. Nucl. Med. *54*, 83–89.
7. Lewis, J.S., Windhorst, A.D., and Zeglis, B.M. (2019). Radiopharmaceutical Chemistry (Springer).
8. Blasberg, R.G., and Gelovani, J. (2002). Molecular-genetic imaging: a nuclear medicine-based perspective. Mol. Imaging *1*, 280–300.
9. Gambhir, S.S., Herschman, H.R., Cherry, S.R., Barrio, J.R., Satyamurthy, N., Toyokuni, T., Phelps, M.E., Larson, S.M., Balatoni, J., Finn, R., et al. (2000). Imaging transgene expression with radionuclide imaging technologies. Neoplasia *2*, 118–138.
10. Yaghoubi, S.S., and Gambhir, S.S. (2006). PET imaging of herpes simplex virus type 1 thymidine kinase (*HSV1-tk*) or mutant *HSV1-sr39tk* reporter gene expression in mice and humans using [^{18}F]FHBG. Nat. Protoc. *1*, 3069–3075.
11. Pillarsetty, N., Cai, S., Ageyeva, L., Finn, R.D., and Blasberg, R.G. (2006). Synthesis and evaluation of [^{18}F] labeled pyrimidine nucleosides for positron emission tomography imaging of herpes simplex virus 1 thymidine kinase gene expression. J. Med. Chem. *49*, 5377–5381.
12. Zhang, H., Huang, R., Pillarsetty, N., Thorek, D.L., Vaidyanathan, G., Serganova, I., Blasberg, R.G., and Lewis, J.S. (2014). Synthesis and evaluation of ^{18}F-labeled benzylguanidine analogs for targeting the human norepinephrine transporter. Eur. J. Nucl. Med. Mol. Imaging *41*, 322–332.
13. Serganova, I., Moroz, E., Vider, J., Gogiberidze, G., Moroz, M., Pillarsetty, N., Doubrovin, M., Minn, A., Thaler, H.T., Massague, J., et al. (2009). Multimodality imaging of TGFβ signaling in breast cancer metastases. FASEB J. *23*, 2662–2672.
14. Dobrenkov, K., Olszewska, M., Likar, Y., Shenker, L., Gunset, G., Cai, S., Pillarsetty, N., Hricak, H., Sadelain, M., and Ponomarev, V. (2008). Monitoring the efficacy of adoptively transferred prostate cancer-targeted human T lymphocytes with PET and bioluminescence imaging. J. Nucl. Med. *49*, 1162–1170.
15. Hong, H., Zhang, Y., and Cai, W. (2010). In vivo imaging of RNA interference. J. Nucl. Med. *51*, 169–172.
16. Adonai, N., Adonai, N., Nguyen, K.N., Walsh, J., Iyer, M., Toyokuni, T., Phelps, M.E., McCarthy, T., McCarthy, D.W., and Gambhir, S.S. (2002). Ex vivo cell labeling with ^{64}Cu-pyruvaldehyde-bis(N^4-methylthiosemicarbazone) for imaging cell trafficking in mice with positron-emission tomography. Proc. Natl. Acad. Sci. USA *99*, 3030–3035.
17. Bansal, A., Pandey, M.K., Demirhan, Y.E., Nesbitt, J.J., Crespo-Diaz, R.J., Terzic, A., Behfar, A., and DeGrado, T.R. (2015). Novel ^{89}Zr cell labeling approach for PET-based cell trafficking studies. EJNMMI Res. *5*, 19.
18. Kircher, M.F., Allport, J.R., Graves, E.E., Love, V., Josephson, L., Lichtman, A.H., and Weissleder, R. (2003). In vivo high resolution three-dimensional imaging of antigen-specific cytotoxic T-lymphocyte trafficking to tumors. Cancer Res. *63*, 6838–6846.
19. Read, E.J., Keenan, A.M., Carter, C.S., Yolles, P.S., and Davey, R.J. (1990). In vivo traffic of indium-111-oxine labeled human lymphocytes collected by automated apheresis. J. Nucl. Med. *31*, 999–1006.
20. Becker, W., Schomann, E., Fischbach, W., Börner, W., and Gruner, K.R. (1988). Comparison of ^{99}Tcm-HMPAO and ^{111}In-oxine labelled granulocytes in man: first clinical results. Nucl. Med. Commun. *9*, 435–447.
21. Daldrup-Link, H.E., Golovko, D., Ruffell, B., Denardo, D.G., Castaneda, R., Ansari, C., Rao, J., Tikhomirov, G.A., Wendland, M.F., Corot, C., and Coussens, L.M. (2011). MRI of tumor-associated macrophages with clinically applicable iron oxide nanoparticles. Clin. Cancer Res. *17*, 5695–5704.
22. Pérez-Medina, C., Tang, J., Abdel-Atti, D., Hogstad, B., Merad, M., Fisher, E.A., Fayad, Z.A., Lewis, J.S., Mulder, W.J., and Reiner, T. (2015). PET imaging of tumor-associated macrophages with ^{89}Zr-labeled high-density lipoprotein nanoparticles. J. Nucl. Med. *56*, 1272–1277.
23. Tarkin, J.M., Joshi, F.R., and Rudd, J.H. (2014). PET imaging of inflammation in atherosclerosis. Nat. Rev. Cardiol. *11*, 443–457.
24. Kang, S., Lee, H.W., Jeon, Y.H., Singh, T.D., Choi, Y.J., Park, J.Y., Kim, J.S., Lee, H., Hong, K.S., Lee, I., et al. (2015). Combined fluorescence and magnetic resonance imaging of primary macrophage migration to sites of acute inflammation using near-infrared fluorescent magnetic nanoparticles. Mol. Imaging Biol. *17*, 643–651.
25. Nahrendorf, M., Zhang, H., Hembrador, S., Panizzi, P., Sosnovik, D.E., Aikawa, E., Libby, P., Swirski, F.K., and Weissleder, R. (2008). Nanoparticle PET-CT imaging of macrophages in inflammatory atherosclerosis. Circulation *117*, 379–387.
26. Grimm, J., Kircher, M.F., and Weissleder, R. (2007). [Cell tracking. Principles and applications]. Radiologe *47*, 25–33.
27. Aicher, A., Brenner, W., Zuhayra, M., Badorff, C., Massoudi, S., Assmus, B., Eckey, T., Henze, E., Zeiher, A.M., and Dimmeler, S. (2003). Assessment of the tissue distribution of transplanted human endothelial progenitor cells by radioactive labeling. Circulation *107*, 2134–2139.
28. Brenner, W., Aicher, A., Eckey, T., Massoudi, S., Zuhayra, M., Koehl, U., Heeschen, C., Kampen, W.U., Zeiher, A.M., Dimmeler, S., and Henze, E. (2004). ^{111}In-labeled CD34$^+$ hematopoietic progenitor cells in a rat myocardial infarction model. J. Nucl. Med. *45*, 512–518.
29. Zhou, R., Thomas, D.H., Qiao, H., Bal, H.S., Choi, S.R., Alavi, A., Ferrari, V.A., Kung, H.F., and Acton, P.D. (2005). In vivo detection of stem cells grafted in infarcted rat myocardium. J. Nucl. Med. *46*, 816–822.
30. Pittet, M.J., Grimm, J., Berger, C.R., Tamura, T., Wojtkiewicz, G., Nahrendorf, M., Romero, P., Swirski, F.K., and Weissleder, R. (2007). In vivo imaging of T cell delivery to tumors after adoptive transfer therapy. Proc. Natl. Acad. Sci. USA *104*, 12457–12461.
31. Blocklet, D., Toungouz, M., Kiss, R., Lambermont, M., Velu, T., Duriau, D., Goldman, M., and Goldman, S. (2003). ^{111}In-oxine and ^{99m}Tc-HMPAO labelling of antigen-loaded dendritic cells: in vivo imaging and influence on motility and actin content. Eur. J. Nucl. Med. Mol. Imaging *30*, 440–447.
32. Bennink, R.J., Hamann, J., de Bruin, K., ten Kate, F.J., van Deventer, S.J., and te Velde, A.A. (2005). Dedicated pinhole SPECT of intestinal neutrophil recruitment in a mouse model of dextran sulfate sodium-induced colitis. J. Nucl. Med. *46*, 526–531.
33. de Vries, E.F., Roca, M., Jamar, F., Israel, O., and Signore, A.; Inflammation/Infection Taskgroup of the European Association of Nuclear Medicine (2010). Guidelines for the labelling of leucocytes with ^{99m}Tc-HMPAO. Eur. J. Nucl. Med. Mol. Imaging *37*, 842–848.
34. Lukawska, J.J., Livieratos, L., Sawyer, B.M., Lee, T., O'Doherty, M., Blower, P.J., Kofi, M., Ballinger, J.R., Corrigan, C.J., Gnanasegaran, G., et al. (2014). Imaging inflammation in asthma: real time, differential tracking of human neutrophil and eosinophil migration in allergen challenged, atopic asthmatics in vivo. EBioMedicine *1*, 173–180.
35. Lukawska, J.J., Livieratos, L., Sawyer, B.M., Lee, T., O'Doherty, M., Blower, P.J., Kofi, M., Ballinger, J.R., Corrigan, C.J., Gnanasegaran, G., et al. (2014). Real-time differential tracking of human neutrophil and eosinophil migration in vivo. J. Allergy Clin. Immunol. *133*, 233–239.e1.
36. Stojanov, K., de Vries, E.F., Hoekstra, D., van Waarde, A., Dierckx, R.A., and Zuhorn, I.S. (2012). ^{18F}FDG labeling of neural stem cells for in vivo cell tracking with positron emission tomography: inhibition of tracer release by phloretin. Mol. Imaging *11*, 1–12.
37. Meier, R., Piert, M., Piontek, G., Rudelius, M., Oostendorp, R.A., Senekowitsch-Schmidtke, R., Henning, T.D., Wels, W.S., Uherek, C., Rummeny, E.J., and Daldrup-Link, H.E. (2008). Tracking of ^{18F}FDG-labeled natural killer cells to HER2/neu-positive tumors. Nucl. Med. Biol. *35*, 579–588.

38. Zhang, Y., Dasilva, J.N., Hadizad, T., Thorn, S., Kuraitis, D., Renaud, J.M., Ahmadi, A., Kordos, M., Dekemp, R.A., Beanlands, R.S., et al. (2012). ^{18}F-FDG cell labeling may underestimate transplanted cell homing: more accurate, efficient, and stable cell labeling with hexadecyl-4-[^{18}F]fluorobenzoate for in vivo tracking of transplanted human progenitor cells by positron emission tomography. Cell Transplant. *21*, 1821–1835.

39. Swirski, F.K., Pittet, M.J., Kircher, M.F., Aikawa, E., Jaffer, F.A., Libby, P., and Weissleder, R. (2006). Monocyte accumulation in mouse atherogenesis is progressive and proportional to extent of disease. Proc. Natl. Acad. Sci. USA *103*, 10340–10345.

40. Avila-Rodriguez, M.A., Rios, C., Carrasco-Hernandez, J., Manrique-Arias, J.C., Martinez-Hernandez, R., García-Pérez, F.O., Jalilian, A.R., Martinez-Rodriguez, E., Romero-Piña, M.E., and Diaz-Ruiz, A. (2017). Biodistribution and radiation dosimetry of [^{64}Cu]copper dichloride: first-in-human study in healthy volunteers. EJNMMI Res. *7*, 98.

41. Sato, N., Stringaris, K., Davidson-Moncada, J.K., Reger, R., Adler, S.S., Dunbar, C., Choyke, P.L., and Childs, R.W. (2020). *In vivo* tracking of adoptively transferred natural killer cells in rhesus macaques using ^{89}zirconium-oxine cell labeling and PET imaging. Clin. Cancer Res. *26*, 2573–2581.

42. Weist, M.R., Starr, R., Aguilar, B., Chea, J., Miles, J.K., Poku, E., Gerdts, E., Yang, X., Priceman, S.J., Forman, S.J., et al. (2018). PET of adoptively transferred chimeric antigen receptor T cells with ^{89}Zr-oxine. J. Nucl. Med. *59*, 1531–1537.

43. Sato, N., Wu, H., Asiedu, K.O., Szajek, L.P., Griffiths, G.L., and Choyke, P.L. (2015). ^{89}Zr-oxine complex PET cell imaging in monitoring cell-based therapies. Radiology *275*, 490–500.

44. Man, F., Lim, L., Volpe, A., Gabizon, A., Shmeeda, H., Draper, B., Parente-Pereira, A.C., Maher, J., Blower, P.J., Fruhwirth, G.O., and T M de Rosales, R. (2019). In vivo pet tracking of ^{89}Zr-labeled Vγ9Vδ2 T cells to mouse xenograft breast tumors activated with liposomal alendronate. Mol. Ther. *27*, 219–229.

45. Botti, C., Negri, D.R., Seregni, E., Ramakrishna, V., Arienti, F., Maffioli, L., Lombardo, C., Bogni, A., Pascali, C., Crippa, F., et al. (1997). Comparison of three different methods for radiolabelling human activated T lymphocytes. Eur. J. Nucl. Med. *24*, 497–504.

46. Rogers, B.E., McLean, S.F., Kirkman, R.L., Della Manna, D., Bright, S.J., Olsen, C.C., Myracle, A.D., Mayo, M.S., Curiel, D.T., and Buchsbaum, D.J. (1999). In vivo localization of [^{111}In]-DTPA-D-Phe1-octreotide to human ovarian tumor xenografts induced to express the somatostatin receptor subtype 2 using an adenoviral vector. Clin. Cancer Res. *5*, 383–393.

47. Shulkin, B.L., Shapiro, B., Tobes, M.C., Shen, S.W., Wieland, D.M., Meyers, L.J., Lee, H.T., Petry, N.A., Sisson, J.C., and Beierwaltes, W.H. (1986). Iodine-123-4-amino-3-iodobenzylguanidine, a new sympathoadrenal imaging agent: comparison with iodine-123 metaiodobenzylguanidine. J. Nucl. Med. *27*, 1138–1142.

48. Glowniak, J.V., Kilty, J.E., Amara, S.G., Hoffman, B.J., and Turner, F.E. (1993). Evaluation of metaiodobenzylguanidine uptake by the norepinephrine, dopamine and serotonin transporters. J. Nucl. Med. *34*, 1140–1146.

49. Russell, S.J., and Peng, K.W. (2007). Viruses as anticancer drugs. Trends Pharmacol. Sci. *28*, 326–333.

50. Russell, S.J., Peng, K.W., and Bell, J.C. (2012). Oncolytic virotherapy. Nat. Biotechnol. *30*, 658–670.

51. Mineta, T., Rabkin, S.D., Yazaki, T., Hunter, W.D., and Martuza, R.L. (1995). Attenuated multi-mutated herpes simplex virus-1 for the treatment of malignant gliomas. Nat. Med. *1*, 938–943.

52. Kooby, D.A., Carew, J.F., Halterman, M.W., Mack, J.E., Bertino, J.R., Blumgart, L.H., Federoff, H.J., and Fong, Y. (1999). Oncolytic viral therapy for human colorectal cancer and liver metastases using a multi-mutated herpes simplex virus type-1 (G207). FASEB J. *13*, 1325–1334.

53. Yoon, S.S., Nakamura, H., Carroll, N.M., Bode, B.P., Chiocca, E.A., and Tanabe, K.K. (2000). An oncolytic herpes simplex virus type 1 selectively destroys diffuse liver metastases from colon carcinoma. FASEB J. *14*, 301–311.

54. Carew, J.F., Kooby, D.A., Halterman, M.W., Federoff, H.J., and Fong, Y. (1999). Selective infection and cytolysis of human head and neck squamous cell carcinoma with sparing of normal mucosa by a cytotoxic herpes simplex virus type 1 (G207). Hum. Gene Ther. *10*, 1599–1606.

55. Toyoizumi, T., Mick, R., Abbas, A.E., Kang, E.H., Kaiser, L.R., and Molnar-Kimber, K.L. (1999). Combined therapy with chemotherapeutic agents and herpes simplex virus type 1 ICP34.5 mutant (HSV-1716) in human non-small cell lung cancer. Hum. Gene Ther. *10*, 3013–3029.

56. Advani, S.J., Chung, S.M., Yan, S.Y., Gillespie, G.Y., Markert, J.M., Whitley, R.J., Roizman, B., and Weichselbaum, R.R. (1999). Replication-competent, nonneuroinvasive genetically engineered herpes virus is highly effective in the treatment of therapy-resistant experimental human tumors. Cancer Res. *59*, 2055–2058.

57. Bennett, J.J., Tjuvajev, J., Johnson, P., Doubrovin, M., Akhurst, T., Malholtra, S., Hackman, T., Balatoni, J., Finn, R., Larson, S.M., et al. (2001). Positron emission tomography imaging for herpes virus infection: Implications for oncolytic viral treatments of cancer. Nat. Med. *7*, 859–863.

58. Peñuelas, I., Mazzolini, G., Boán, J.F., Sangro, B., Martí-Climent, J., Ruiz, M., Ruiz, J., Satyamurthy, N., Qian, C., Barrio, J.R., et al. (2005). Positron emission tomography imaging of adenoviral-mediated transgene expression in liver cancer patients. Gastroenterology *128*, 1787–1795.

59. Moolten, F.L. (1994). Drug sensitivity ("suicide") genes for selective cancer chemotherapy. Cancer Gene Ther. *1*, 279–287.

60. Miller, A., and Russell, S.J. (2016). The use of the NIS reporter gene for optimizing oncolytic virotherapy. Expert Opin. Biol. Ther. *16*, 15–32.

61. Hasegawa, K., Pham, L., O'Connor, M.K., Federspiel, M.J., Russell, S.J., and Peng, K.W. (2006). Dual therapy of ovarian cancer using measles viruses expressing carcinoembryonic antigen and sodium iodide symporter. Clin. Cancer Res. *12*, 1868–1875.

62. Dingli, D., Peng, K.W., Harvey, M.E., Greipp, P.R., O'Connor, M.K., Cattaneo, R., Morris, J.C., and Russell, S.J. (2004). Image-guided radiovirotherapy for multiple myeloma using a recombinant measles virus expressing the thyroidal sodium iodide symporter. Blood *103*, 1641–1646.

63. Liu, C., Russell, S.J., and Peng, K.W. (2010). Systemic therapy of disseminated myeloma in passively immunized mice using measles virus-infected cell carriers. Mol. Ther. *18*, 1155–1164.

64. Msaouel, P., Iankov, I.D., Allen, C., Aderca, I., Federspiel, M.J., Tindall, D.J., Morris, J.C., Koutsilieris, M., Russell, S.J., and Galanis, E. (2009). Noninvasive imaging and radiovirotherapy of prostate cancer using an oncolytic measles virus expressing the sodium iodide symporter. Mol. Ther. *17*, 2041–2048.

65. Blechacz, B., Splinter, P.L., Greiner, S., Myers, R., Peng, K.W., Federspiel, M.J., Russell, S.J., and LaRusso, N.F. (2006). Engineered measles virus as a novel oncolytic viral therapy system for hepatocellular carcinoma. Hepatology *44*, 1465–1477.

66. Penheiter, A.R., Wegman, T.R., Classic, K.L., Dingli, D., Bender, C.E., Russell, S.J., and Carlson, S.K. (2010). Sodium iodide symporter (NIS)-mediated radiovirotherapy for pancreatic cancer. AJR Am. J. Roentgenol. *195*, 341–349.

67. Merron, A., Peerlinck, I., Martin-Duque, P., Burnet, J., Quintanilla, M., Mather, S., Hingorani, M., Harrington, K., Iggo, R., and Vassaux, G. (2007). SPECT/CT imaging of oncolytic adenovirus propagation in tumours in vivo using the Na/I symporter as a reporter gene. Gene Ther. *14*, 1731–1738.

68. Dingli, D., Diaz, R.M., Bergert, E.R., O'Connor, M.K., Morris, J.C., and Russell, S.J. (2003). Genetically targeted radiotherapy for multiple myeloma. Blood *102*, 489–496.

69. Likar, Y., Zurita, J., Dobrenkov, K., Shenker, L., Cai, S., Neschadim, A., Medin, J.A., Sadelain, M., Hricak, H., and Ponomarev, V. (2010). A new pyrimidine-specific reporter gene: a mutated human deoxycytidine kinase suitable for PET during treatment with acycloguanosine-based cytotoxic drugs. J. Nucl. Med. *51*, 1395–1403.

70. McCracken, M.N., Vatakis, D.N., Dixit, D., McLaughlin, J., Zack, J.A., and Witte, O.N. (2015). Noninvasive detection of tumor-infiltrating T cells by PET reporter imaging. J. Clin. Invest. *125*, 1815–1826.

71. Vedvyas, Y., Shevlin, E., Zaman, M., Min, I.M., Amor-Coarasa, A., Park, S., Park, S., Kwon, K.W., Smith, T., Luo, Y., et al. (2016). Longitudinal PET imaging demonstrates biphasic CAR T cell responses in survivors. JCI Insight *1*, e90064.

72. Moroz, M.A., Zhang, H., Lee, J., Moroz, E., Zurita, J., Shenker, L., Serganova, I., Blasberg, R., and Ponomarev, V. (2015). Comparative analysis of T cell imaging with human nuclear reporter genes. J. Nucl. Med. *56*, 1055–1060.

73. Miyagawa, T., Gogiberidze, G., Serganova, I., Cai, S., Balatoni, J.A., Thaler, H.T., Ageyeva, L., Pillarsetty, N., Finn, R.D., and Blasberg, R.G. (2008). Imaging of HSV-*tk* reporter gene expression: comparison between [^{18}F]FEAU, [^{18}F]FFEAU, and other imaging probes. J. Nucl. Med. *49*, 637–648.

74. Rao, V.P., Miyagi, N., Ricci, D., Carlson, S.K., Morris, J.C., 3rd, Federspiel, M.J., Bailey, K.R., Russell, S.J., and McGregor, C.G. (2007). Sodium iodide symporter (hNIS) permits molecular imaging of gene transduction in cardiac transplantation. Transplantation *84*, 1662–1666.

75. Mayer-Kuckuk, P., Doubrovin, M., Bidaut, L., Budak-Alpdogan, T., Cai, S., Hubbard, V., Alpdogan, O., van den Brink, M., Bertino, J.R., Blasberg, R.G., et al. (2006). Molecular imaging reveals skeletal engraftment sites of transplanted bone marrow cells. Cell Transplant. *15*, 75–82.

76. Ashmore-Harris, C., Blackford, S.J., Grimsdell, B., Kurtys, E., Glatz, M.C., Rashid, T.S., and Fruhwirth, G.O. (2019). Reporter gene-engineering of human induced pluripotent stem cells during differentiation renders in vivo traceable hepatocyte-like cells accessible. Stem Cell Res. (Amst.) *41*, 101599.

77. Koehne, G., Doubrovin, M., Doubrovina, E., Zanzonico, P., Gallardo, H.F., Ivanova, A., Balatoni, J., Teruya-Feldstein, J., Heller, G., May, C., et al. (2003). Serial in vivo imaging of the targeted migration of human HSV-TK-transduced antigen-specific lymphocytes. Nat. Biotechnol. *21*, 405–413.

78. Dotti, G., Tian, M., Savoldo, B., Najjar, A., Cooper, L.J., Jackson, J., Smith, A., Mawlawi, O., Uthamanthil, R., Borne, A., et al. (2009). Repetitive noninvasive monitoring of HSV1-tk-expressing T cells intravenously infused into nonhuman primates using positron emission tomography and computed tomography with ^{18}F-FEAU. Mol. Imaging *8*, 230–237.

79. Doubrovin, M.M., Doubrovina, E.S., Zanzonico, P., Sadelain, M., Larson, S.M., and O'Reilly, R.J. (2007). In vivo imaging and quantitation of adoptively transferred human antigen-specific T cells transduced to express a human norepinephrine transporter gene. Cancer Res. *67*, 11959–11969.

80. Volpe, A., Lang, C., Lim, L., Man, F., Kurtys, E., Ashmore-Harris, C., Johnson, P., Skourti, E., de Rosales, R.T.M., and Fruhwirth, G.O. (2020). Spatiotemporal PET imaging reveals differences in CAR-T tumor retention in triple-negative breast cancer models. Mol. Ther. *28*, 2271–2285.

81. O'Doherty, J., Jauregui-Osoro, M., Brothwood, T., Szyszko, T., Marsden, P.K., O'Doherty, M.J., Cook, G.J.R., Blower, P.J., and Lewington, V. (2017). ^{18}F-tetrafluoroborate, a PET probe for imaging sodium/iodide symporter expression: whole-body biodistribution, safety, and radiation dosimetry in thyroid cancer patients. J. Nucl. Med. *58*, 1666–1671.

82. Ponomarev, V., Doubrovin, M., Lyddane, C., Beresten, T., Balatoni, J., Bornman, W., Finn, R., Akhurst, T., Larson, S., Blasberg, R., et al. (2001). Imaging TCR-dependent NFAT-mediated T-cell activation with positron emission tomography in vivo. Neoplasia *3*, 480–488.

83. Mayer-Kuckuk, P., Banerjee, D., Malhotra, S., Doubrovin, M., Iwamoto, M., Akhurst, T., Balatoni, J., Bornmann, W., Finn, R., Larson, S., et al. (2002). Cells exposed to antifolates show increased cellular levels of proteins fused to dihydrofolate reductase: a method to modulate gene expression. Proc. Natl. Acad. Sci. USA *99*, 3400–3405.

84. Alauddin, M.M., Conti, P.S., Mazza, S.M., Hamzeh, F.M., and Lever, J.R. (1996). 9-[(3-[^{18}F]-fluoro-1-hydroxy-2-propoxy)methyl]guanine ([^{18}F]-FHPG): a potential imaging agent of viral infection and gene therapy using PET. Nucl. Med. Biol. *23*, 787–792.

85. Alauddin, M.M., and Conti, P.S. (1998). Synthesis and preliminary evaluation of 9-(4-[^{18}F]-fluoro-3-hydroxymethylbutyl)guanine ([^{18}F]FHBG): a new potential imaging agent for viral infection and gene therapy using PET. Nucl. Med. Biol. *25*, 175–180.

86. Gambhir, S.S., Barrio, J.R., Phelps, M.E., Iyer, M., Namavari, M., Satyamurthy, N., Wu, L., Green, L.A., Bauer, E., MacLaren, D.C., et al. (1999). Imaging adenoviral-directed reporter gene expression in living animals with positron emission tomography. Proc. Natl. Acad. Sci. USA *96*, 2333–2338.

87. Gambhir, S.S., Bauer, E., Black, M.E., Liang, Q., Kokoris, M.S., Barrio, J.R., Iyer, M., Namavari, M., Phelps, M.E., and Herschman, H.R. (2000). A mutant herpes simplex virus type 1 thymidine kinase reporter gene shows improved sensitivity for imaging reporter gene expression with positron emission tomography. Proc. Natl. Acad. Sci. USA *97*, 2785–2790.

88. Haberkorn, U., Khazaie, K., Morr, I., Altmann, A., Müller, M., and van Kaick, G. (1998). Ganciclovir uptake in human mammary carcinoma cells expressing herpes simplex virus thymidine kinase. Nucl. Med. Biol. *25*, 367–373.

89. Alauddin, M.M., Shahinian, A., Park, R., Tohme, M., Fissekis, J.D., and Conti, P.S. (2004). Synthesis of 2′-deoxy-2′-[^{18}F]fluoro-5-bromo-1-β-D-arabinofuranosyluracil ([^{18}F]-FBAU) and 2′-deoxy-2′-[^{18}F]fluoro-5-chloro-1-β-D-arabinofuranosyl-uracil ([^{18}F]-FCAU), and their biological evaluation as markers for gene expression. Nucl. Med. Biol. *31*, 399–405.

90. Fuchigami, T., Haywood, T., Gowrishankar, G., Anders, D., Namavari, M., Wardak, M., and Gambhir, S.S. (2020). Synthesis and characterization of 9-(4-[^{18}F]fluoro-3-(hydroxymethyl)butyl)-2-(phenylthio)-6-oxopurine as a novel PET agent for mutant herpes simplex virus type 1 thymidine kinase reporter gene imaging. Mol. Imaging Biol. *22*, 1151–1160.

91. Yaghoubi, S., Barrio, J.R., Dahlbom, M., Iyer, M., Namavari, M., Satyamurthy, N., Goldman, R., Herschman, H.R., Phelps, M.E., and Gambhir, S.S. (2001). Human pharmacokinetic and dosimetry studies of [^{18}F]FHBG: a reporter probe for imaging herpes simplex virus type-1 thymidine kinase reporter gene expression. J. Nucl. Med. *42*, 1225–1234.

92. Tjuvajev, J.G., Doubrovin, M., Akhurst, T., Cai, S., Balatoni, J., Alauddin, M.M., Finn, R., Bornmann, W., Thaler, H., Conti, P.S., and Blasberg, R.G. (2002). Comparison of radiolabeled nucleoside probes (FIAU, FHBG, and FHPG) for PET imaging of HSV1-*tk* gene expression. J. Nucl. Med. *43*, 1072–1083.

93. Yaghoubi, S.S., Jensen, M.C., Satyamurthy, N., Budhiraja, S., Paik, D., Czernin, J., and Gambhir, S.S. (2009). Noninvasive detection of therapeutic cytolytic T cells with ^{18}F-FHBG PET in a patient with glioma. Nat. Clin. Pract. Oncol. *6*, 53–58.

94. Keu, K.V., Witney, T.H., Yaghoubi, S., Rosenberg, J., Kurien, A., Magnusson, R., Williams, J., Habte, F., Wagner, J.R., Forman, S., et al. (2017). Reporter gene imaging of targeted T cell immunotherapy in recurrent glioma. Sci. Transl. Med. *9*, eaag2196.

95. Likar, Y., Dobrenkov, K., Olszewska, M., Shenker, L., Cai, S., Hricak, H., and Ponomarev, V. (2009). PET imaging of HSV1-tk mutants with acquired specificity toward pyrimidine- and acycloguanosine-based radiotracers. Eur. J. Nucl. Med. Mol. Imaging *36*, 1273–1282.

96. Kircher, M.F., Gambhir, S.S., and Grimm, J. (2011). Noninvasive cell-tracking methods. Nat. Rev. Clin. Oncol. *8*, 677–688.

97. Minn, I., Menezes, M.E., Sarkar, S., Yarlagadda, K., Das, S.K., Emdad, L., Sarkar, D., Fisher, P.B., and Pomper, M.G. (2014). Molecular-genetic imaging of cancer. Adv. Cancer Res. *124*, 131–169.

98. Hoekstra, M.E., Dijkgraaf, F.E., Schumacher, T.N., and Rohr, J.C. (2015). Assessing T lymphocyte function and differentiation by genetically encoded reporter systems. Trends Immunol. *36*, 392–400.

99. Cherry, S.R., Jones, T., Karp, J.S., Qi, J., Moses, W.W., and Badawi, R.D. (2018). Total-body PET: maximizing sensitivity to create new opportunities for clinical research and patient care. J. Nucl. Med. *59*, 3–12.

100. Shao, Y., Cherry, S.R., Farahani, K., Meadors, K., Siegel, S., Silverman, R.W., and Marsden, P.K. (1997). Simultaneous PET and MR imaging. Phys. Med. Biol. *42*, 1965–1970.

101. Slates, R.B., Farahani, K., Shao, Y., Marsden, P.K., Taylor, J., Summers, P.E., Williams, S., Beech, J., and Cherry, S.R. (1999). A study of artefacts in simultaneous PET and MR imaging using a prototype MR compatible PET scanner. Phys. Med. Biol. *44*, 2015–2027.